Misincorporation and Stalling at O^6-Methylguanine and O^6-Benzylguanine: Evidence for Inactive Polymerase Complexes†

Adrienne M. Woodside‡ and F. Peter Guengerich*

Department of Biochemistry and Center in Molecular Toxicology, Vanderbilt University School of Medicine, Nashville, Tennessee 37232-0146

Received July 17, 2001; Revised Manuscript Received September 26, 2001

ABSTRACT: Many DNA−carcinogen adducts not only compromise polymerase fidelity but also inhibit replication. This polymerase stalling or "idling" may then contribute to misincorporations if the polymerase is not completely blocked, such as the G:C to A:T mutations caused by O^6-substituted guanines. Kinetic experiments were conducted to address the mechanism of polymerase stalling of T7 DNA polymerase exo$^-$ (T7$^-$) and HIV-1 reverse transcriptase (RT) during replication of primer/template DNA containing guanine (G), O^6-methylguanine (O^6-MeG), or O^6-benzylguanine (O^6-BzG), thus, extending work presented in the preceding paper in this issue [Woodside, A. M., and Guengerich, F. P. (2002) *Biochemistry 41*, 1027−1038]. Substitution of a thio-substituted dNTP did not appear to strongly affect the chemistry of phosphodiester bond formation because the rate decreased <3-fold. Although the K_d^{DNA} for "productive" binding increased for both T7$^-$ and RT as a function of the O6 substituent, fluorescence titrations indicate that the ground-state DNA binding was not affected for O^6-alkylG substrates. DNA dissociation rates (k_{off}) did not differ between unmodified and adduct-containing substrates. The presence of the correct nucleotide stabilized E•DNA interactions, resulting in a 10-fold slower k_{off}. Pre-steady-state experiments done in the presence of trap DNA revealed two rates of incorporation at the adduct, differing ∼100-fold. Kinetic modeling fit the experimentally determined data (i.e., low burst amplitude at the adduct) only if the mechanism included an inactive E•DNA•dNTP complex. In summary, several lines of evidence indicate that the existence of a nonproductive polymerase complex best explains polymerase kinetics at DNA−carcinogen adducts, specifically O^6-alkylguanine.

Polymerases rapidly replicate the cellular genome with high accuracy. Replication is highly regulated to ensure high fidelity of the polymerase—several studies indicate that the error rate in a human cell is 1.4 ± 10^{-10} mutations/base pair/cell generation (*1*). *Escherichia coli* DNA is replicated at an estimated rate of 1000 nucleotides s^{-1} (*2*). Thus, polymerases that replicate the genome are highly processive enzymes, that is, they add hundreds of nucleotides to the nascent DNA chain before dissociating. Repair polymerases are more distributive in nature, adding a few nucleotides before releasing the DNA.

Regardless of processivity, most polymerases employ the same general mechanism of DNA replication and phosphodiester bond formation (*3*−*6*). The general polymerase mechanism includes the following steps: the polymerase binds DNA, the E•DNA[1] complex binds dNTP, and then a conformational change occurs prior to phosphodiester bond formation. Following bond formation, the enzyme conformation relaxes to release pyrophosphate. During DNA replication, the conformational change after dNTP binding is believed to be rate-limiting (*3*, *4*, *7*). Evidence from crystal structures suggests that after the correct dNTP-Mg^{2+} binds, a conformational change in the "fingers domain" occurs. This change in protein conformation ensures a tight fit in the active site, thus, changing the initial E•DNA•dNTP complex into a "closed" ternary complex (*8*, *9*). The "closed" ternary complex permits alignment of the primer 3′-hydroxyl with the α-phosphate of the incoming dNTP, facilitating the rapid chemistry of bond formation (*7*, *10*).

This minimal mechanism of polymerization explains the microscopic steps of polymerization when a polymerase replicates normal DNA. The mechanism may not fully explain the altered kinetics of a polymerase encounter with unusual replication substrates, such as DNA secondary

† This work was supported in part by United States Public Health Service (USPHS) Grants R35 CA44353, R01 ES10546, and P30 ES00267.

‡ Formerly Adrienne N. Mican. Supported in part by USPHS T32 ES07028.

* To whom correspondence should be addressed at the Department of Biochemistry and Center in Molecular Toxicology, Vanderbilt University School of Medicine, 638 Robinson Research Building, 23rd and Pierce Avenues, Nashville, TN 37232-0146. Telephone: (615) 322-2261. Fax: (615) 322-3141. E-mail: guengerich@toxicology.mc.vanderbilt.edu.

[1] Abbreviations: G, guanine; C, cytosine; T, thymine; O^6-alkylG, O^6-alkylguanine; O^6-MeG, O^6-methylguanine; O^6-BzG, O^6-benzylguanine; FAM, 6-carboxyfluorescein; Bz, benzyl; dG, 2′-deoxyguanosine; 8oxoG, 8-oxo-7,8-dihydroguanine; 8-oxodGTP, 8-oxoG 5′-triphosphate; dCTPαS, 2′-deoxycytidine 5′-*O*-(1-thiotriphosphate); dTTPαS, 2′-deoxythymidine 5′-*O*-(1-thiotriphosphate); E, enzyme (used when describing complexes that include the polymerase); T7$^-$, T7 DNA polymerase exo$^-$; RT, human immunodeficiency virus-1 reverse transcriptase; Tris, tris(hydroxymethyl)aminomethane; DTT, DL-dithiothreitol; BSA, bovine serum albumin; EDTA, (ethylenedinitrilo)-tetraacetic acid; 1× TBE, 90 mM Tris-borate buffer (pH 8.5) containing 2 mM EDTA.

10.1021/bi011496f CCC: $22.00
Published on Web 12/27/2001

structures (*11*), RNA secondary structures (*12*), DNA−carcinogen adducts (*13*−*15*), or other natural "pause" sites (*16*). Although these unusual substrates can alter polymerase fidelity, polymerase "stalling" or "pausing" may play important biological roles. Secondary structures in DNA and RNA may contribute to transcription attenuation. These secondary structures may also be present in viral genomes, but the reason for this is not clearly understood (*16*). Stalling at DNA−carcinogen adducts may signal for the start of translesion synthesis, which recruits other polymerases to the site of the adduct (*17*, *18*).

Polymerase substrates that cause stalling also affect polymerization kinetics. Increased DNA dissociation, decreased DNA substrate affinity, or inhibition of bond formation (or the rate-limiting conformational change) are theories that have been proposed to explain altered kinetics of unusual polymerase substrates. Pre-steady-state kinetics of incorporation normally exhibits two phases: a burst phase with an amplitude that is stoichiometric with enzyme concentration and a slower linear phase, the rate of which reflects the overall rate-limiting step of DNA dissociation (*3*, *4*). During polymerase stalling, the burst phase is usually attenuated, resulting in a substoichiometric burst amplitude (*11*−*15*).

Some evidence suggests that the reduced burst amplitude may be due to formation of nonproductive complexes, rather than any changes in the rates of dissociation or bond formation (*13*, *14*, *19*). Polymerase binding of altered DNA substrates may result in nonproductive complexes. Phosphodiester bond formation occurs only if the nonproductive polymerase complexes can change conformation and assume a catalytically competent state. In this study, incorporation opposite O^6-MeG and O^6-BzG by T7$^-$ and RT results in biphasic kinetics with reduced burst amplitudes [see preceding paper in this issue (*20*)]. Altered DNA binding affinity, increased DNA dissociation, or a rate-limiting chemistry step do not explain the substoichiometric burst or the pausing/stalling seen in the presence of O^6-alkylG. Experimental evidence and computer simulation suggest that the minimal mechanism of polymerization does not explain the altered kinetics at O^6-alkylG. The existence of a nonproductive complex best explains the kinetics of T7$^-$ and RT observed at these DNA adducts.

EXPERIMENTAL PROCEDURES

Enzymes. T7$^-$ and RT were previously expressed and purified in this laboratory (*21*) using stock plasmids provided by K. A. Johnson (T7$^-$ and thioredoxin, University of Texas, Austin, TX) (*5*, *22*) and S. Hughes (RT, Frederick Cancer Facility, Frederick, MD) (*23*). Protein concentrations for each experiment were determined using ϵ_{280} values of 144 mM^{-1} cm^{-1} for T7$^-$, 13.7 mM^{-1} cm^{-1} for thioredoxin, and 522 mM^{-1} cm^{-1} for RT (*14*). UV spectra were recorded using a Cary 14/OLIS spectrophotometer (On-Line Instrument Systems, Bogart, GA).

Nucleoside Triphosphates. Unlabeled Ultrapure Grade dNTPs were purchased from Amersham-Pharmacia Biotech (Piscataway, NJ), and dCTPαS and dTTPαS were from USB (Cleveland, OH). [γ-^{32}P]ATP was purchased from NEN Life Science (Boston, MA).

Oligonucleotides. All oligonucleotides, except the 36-mer oligonucleotide containing O^6-BzG, were purchased as "trityl-off" oligonucleotides from Midland Certified (Midland, Texas) or Operon Technologies (Alameda, CA). Oligonucleotide purification was performed and purity (>99%) was analyzed as previously described (*20*). The extinction coefficients for the oligonucleotides, determined by the Borer method (*24*), were as follows: 18-FAM-mer, ϵ_{260} = 196 mM^{-1} cm^{-1}; 24-mer, 24dd-mer, ϵ_{260} = 224 mM^{-1} cm^{-1}; 25C-mer, ϵ_{260} = 230 mM^{-1} cm^{-1}; 25T-mer, ϵ_{260} = 232 mM^{-1} cm^{-1}; and 36-mer, ϵ_{260} = 310 mM^{-1} cm^{-1}.

Synthesis of O^6*-Bz-dG Phosphoramidite and Site-specifically Modified 36-*O^6*-BzG-mer.* O^6-Bz-dG phosphoramidite was synthesized using Aldrich chemicals (Milwaukee, WI) according to a previously published procedure (*25*) with slight modification (*20*). The O^6-Bz-dG phosphoramidite was incorporated into a 36-mer oligonucleotide, which was extensively characterized and purified as previously described (*20*).

Buffers and Reaction Conditions for Enzyme Assays. Unless indicated otherwise, all RT reactions were performed at 37 °C (*4*) in 50 mM Tris-HCl buffer (pH 7.5 at 37 °C) containing 50 mM NaCl. All T7$^-$ reactions were performed at 22 °C (*26*). For each experiment, T7$^-$ was reconstituted immediately prior to use. Thioredoxin was prepared separately in buffer containing 5 mM DTT without BSA, and T7$^-$ was prepared in buffer without DTT and BSA. T7$^-$ was then reconstituted so that T7$^-$ and thioredoxin were in a 1:20 molar ratio (*5*) with a final buffer composition of 40 mM Tris-HCl (pH 7.5 at 22 °C), 50 mM NaCl, 1.0 mM EDTA, 10 mM DTT, and 9.5 μg BSA mL^{-1}. All reactions were initiated by addition of dNTP so that the final buffer composition was 50 mM Tris-HCl (pH 7.4 at 22 °C) containing 12.5 mM $MgCl_2$.

Labeling/Annealing. The primer (200 pmol) was 5′-end-labeled using T4 polynucleotide kinase and purified on a Biospin column (Biorad, Hercules, CA). Template (36-mer) and labeled primer (1.5:1 molar ratio) were annealed in 50 mM Tris-HCl buffer (pH 7.4) containing 2 mM β-mercaptoethanol and 5 mM $MgCl_2$ by heating at 90 °C for 10 s and cooling slowly to 22 °C overnight.

Gel Electrophoresis Polymerization Assays with All Four dNTPs. A ^{32}P-labeled 24-mer primer, annealed to either an unmodified or adducted template, was extended in the presence of all four dNTPs (100 μM). Each reaction was initiated by adding an equal volume of dNTPs-Mg^{2+} to a preincubated E•DNA complex (100 nM DNA duplex), yielding an 8 μL reaction volume. After 30 min, reactions were quenched with 2 volumes (16 μL) of 20 mM EDTA (pH 9.4) in 95% formamide (w/v). Samples were run on a denaturing gel containing 8.0 M urea and 16% acrylamide (w/v) (from a 19:1 acrylamide:bisacrylamide solution, AccuGel, National Diagnostics, Atlanta, GA) with 1× TBE buffer. The bands (representing extension of the primer to form the full-length oligonucleotide) were visualized by phosphorimaging using a model 400E PhosphorImager (Molecular Dynamics, Sunnyvale, CA) using Image Software, version 3.3.

Phosphorothioate Analysis of Pre-Steady-State Burst Kinetics. Pre-steady-state kinetics were performed using a model RQF-3 KinTek chemical quench flow (KinTek Corp., Austin, TX) with 50 mM Tris-HCl (pH 7.4) buffer containing 5 mM $MgCl_2$ and 1.0 mM EDTA in the drive syringes. The reaction was initiated when the preequilibrated polymerase•

DNA complex in sample syringe A (12.5 μL) was mixed with either (S_p)-dNTPαS-Mg^{2+} (or for comparison, dNTP-Mg^{2+}) in syringe B (10.9 μL). The reactions were quenched with 0.3 M EDTA (pH 9.4) after reaction times of 5 ms to 5 s. Reactions were combined with 450 μL of formamide-dye solution and run on a denaturing gel, with analysis as described for the gel electrophoresis polymerization reactions. The burst rate was determined via single-exponential analysis from the negative slope of the line of $\ln(P_0 - P_t)$ vs t, where P_0 = product concentration at the end of the burst phase and P_t = product concentration at time, t. The graph was fit to the burst equation $y = A(1 - e^{-k_p t}) + k_{ss}t$, where A = burst amplitude, k_p = pre-steady-state rate of nucleotide incorporation, t = time, and k_{ss} = steady-state rate of nucleotide incorporation (*5*, *27*), and analyzed using GraphPad Prism version 2.0b (San Diego, CA).

Determination of K_d^{DNA}. The K_d^{DNA} for productive binding of T7$^-$ and RT to unmodified and adducted 24-mer/36-mer DNA complexes was determined by pre-steady-state analysis. Polymerase was incubated with increasing concentrations of the substrate DNA in sample syringe A to form an enzyme•DNA complex. Each reaction was initiated by addition of saturating dCTP-Mg^{2+} from sample syringe B and quenched with 0.3 M EDTA after 0.15 s. The maximal burst of polymerization was achieved with little contribution from the slower steady-state phase or multiple turnovers when samples were mixed for 0.15 s; this time point was previously determined to represent the burst amplitudes of a pre-steady-state reaction (*20*). The concentration of product formed at each substrate DNA concentration was determined by gel analysis, and a graph of product (nM 25-mer/36-mer) vs starting concentration (nM 24-mer/36-mer) was plotted. This graph was fit to a quadratic equation in Prism using the equation $[E•DNA] = 0.5(K_d + E_t + D_t) - [0.25(K_d + E_t + D_t)^2 - E_tD_t]^{1/2}$ where E_t = active enzyme concentration, D_t = DNA concentration, and $K_d^{(DNA)}$ = equilibrium dissociation constant of productive DNA binding (*5*, *27*).

Fluorescence Estimation of K_d. Ground-state binding (K_d) of the DNA substrate to RT was determined by fluorescence titration. Varying concentrations of RT (2.5−320 nM) were added to a solution of 50 nM 18-FAM-mer/36-mer and 100 mM Tris-HCl buffer (pH 7.4 at 37 °C) containing 50 mM NaCl and 12.5 mM $MgCl_2$. Fluorescence was monitored using a Varian SF-330 spectrofluorometer (Varian, Walnut Creek, CA) using an excitation wavelength of 492 nm and an emission wavelength of 516 nm. The data were fit to a fluorescence quadratic equation in Prism using the equation $E•DNA = F_o + (A/E_t)(0.5)[(K_d + E_t + D_t) - [(K_d + E_t + D_t)^{2-4*E_t*D_t}]^{1/2}]$ where F_o = initial observed fluorescence, A = amplitude, E_t = enzyme concentration, K_d = DNA dissociation constant from E•DNA, and D_t = DNA concentration (*28*).

DNA Dissociation from Enzyme: k_{off}. The DNA dissociation rate from E•DNA was determined using the rapid quench-flow apparatus. Sample syringe A contained a preincubated solution of RT (350 nM) and unlabeled target DNA (24-mer/36-mer, 50 nM). E•DNA was mixed with ^{32}P-labeled 24-mer/36-G-mer (450 nM) in sample syringe B at time intervals ranging from 0.08 to 30 s. After the sample was mixed for varying times, polymerization was initiated with 200 μM dNTP-Mg^{2+} (in the central drive syringe) for a constant time of 0.25 s. After the sample was expelled from the rapid-quench apparatus, the reaction was mixed rapidly (using a vortex device) in a tube containing 500 μL of 0.3 M EDTA (in 50% formamide, v/v) to stop the reaction. The amount of ^{32}P-labeled 25-mer/36-G-mer product was quantified by gel analysis and plotted against time. The graph was fit to a single-exponential equation in Prism using the equation $y = E_f + E_0(1 - e^{-kt})$ where E_f = free enzyme concentration, E_0 = DNA-bound enzyme concentration, and $k_{(off)}$ = dissociation rate of DNA from E•DNA (*11*). To determine the DNA dissociation rate from E•DNA•dNTP, a preincubated solution of RT (350 nM), unlabeled target DNA (24dd-mer/36-mer, 50 nM), and 100 μM dNTP in sample syringe A was mixed with 25C-mer/36-G-mer in sample syringe B. Formation of ^{32}P-labeled 26-mer/36-G-mer was quantified and plotted against time to determine the DNA dissociation rate from the ternary complex.

Table 1: Oligonucleotides Used in These Studies

18-FAM-mer	**5′ (FAM)**-AGCCAGCCGCAGACGCAG
24-mer	**5′** GCCTCGAGCCAGCCGCAGACGCAG
24dd-mer	**5′** GCCTCGAGCCAGCCGCAGACGCAG^{-H} (dideoxy-terminated)
25C-mer	**5′** GCCTCGAGCCAGCCGCAGACGCAG**C**
25T-mer	**5′** GCCTCGAGCCAGCCGCAGACGCAG**T**
36-mer[a]	**3′** CGGAGCTCGGTCGGCGTCTGCGTC**G***-CTCCTGCGGCT

[a] **G***= unmodified G, O^6-MeG, or O6-BzG.

Pre-Steady-State Kinetics with Excess Unlabeled DNA Trap. DNA trap experiments were performed in the rapid quench-flow apparatus by mixing preequilibrated polymerase•DNA complex (RT, 90 nM; primer/template, 100 nM) in sample syringe A with 200 μM dNTP-Mg^{2+} and unlabeled 24-mer/36-G-mer (3.75 μM) in sample syringe B. Reactions were quenched with 0.3 M EDTA at time intervals ranging from 0.01 to 75 s. Product formation was determined by gel analysis, and a graph of nM product vs time was plotted. The points were fit to a double-exponential equation in Prism using the equation $y = E_tA_1(1 - e^{-k_1 t}) + E_tA_2(1 - e^{-k_2 t})$, where E_t = enzyme concentration, A_1 = enzyme amplitude of fast-phase, k_1 = observed fast-phase rate, A_2 = enzyme amplitude of slow-phase, and k_2 = observed slow-phase rate (*12*−*14*).

Kinetic Simulations. Kinetic simulations were performed using two mechanisms: a minimal mechanism, which has been previously defined for DNA polymerization (*3*, *29*), and a mechanism that includes an alternate ternary complex (*14*). The least-squares fit to the experimentally determined data was calculated using DynaFit (BioKin, Madison, WI) (*30*) run on an iMac computer using a Mac OS 8.5.1 operating system (Apple Computer, Cupertino, CA).

RESULTS

The 24-mer/36-mer duplex with the sequence shown in Table 1 was successfully employed in previous polymerase studies in this laboratory (*21*, *28*). The duplex region of the DNA substrate (24 nucleotides) is sufficiently long enough to accommodate the substrate binding sites of T7$^-$ and RT (*31*, *32*). T7$^-$ and RT were chosen as model polymerases for several reasons, including the need for only one (T7$^-$) or no (RT) accessory proteins, ease of purification and thus availability in large quantities (*5*, *23*), and extensive kinetic

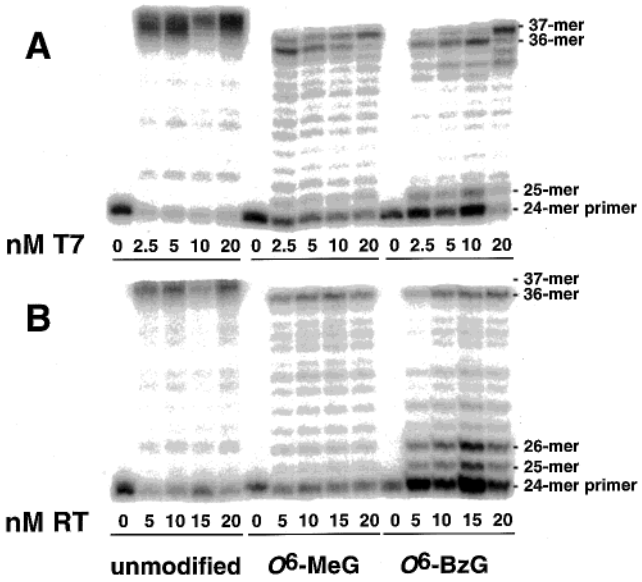

FIGURE 1: Extension of a ^{32}P-labeled 24-mer primer opposite G, O^6-MeG, or O^6-BzG at position 25 by T7$^-$ (A) or RT (B) in the presence of all four dNTPs. Reactions were done in the presence of increasing polymerase concentrations with 100 nM primer/template for 30 min. Following quenching by EDTA, reactions were analyzed by denaturing gel electrophoresis with subsequent phosphorimaging.

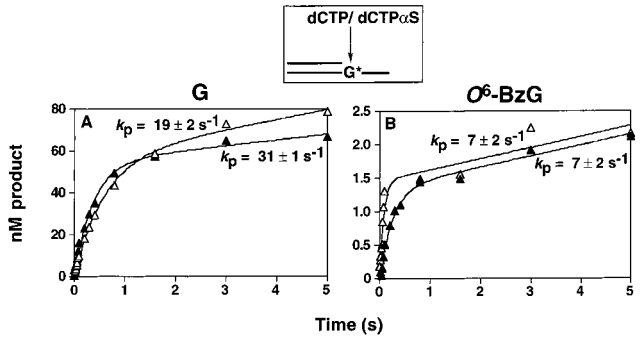

FIGURE 2: Phosphorothioate analysis of pre-steady-state kinetics of correct nucleotide incorporation by T7$^-$. (A) T7$^-$ (23 nM) was incubated with 100 nM 24-mer/36-G-mer in the rapid quench-flow instrument and mixed with 200 μM dCTP (▲) to initiate the reaction. The pre-steady-state rate was determined from the burst equation $y = A(1 - e^{-k_p t}) + k_{ss}t$, as described in the Experimental Procedures, and is indicated in the figure. T7$^-$ (28 nM), preincubated with 100 nM 24-mer/36-G-mer, was mixed with 200 μM dCTPαS (△) to initiate polymerization. (B) T7$^-$ (65 nM) was incubated with 24-mer/36-O^6-BzG-mer to form an E•DNA complex. Polymerization was initiated with the addition of 1.0 mM dCTP (▲). T7$^-$ (66 nM), incubated with 24-mer/36-O^6-BzG-mer, was mixed with 1.0 mM dCTPαS (△) to start the reaction.

characterization with unmodified DNA as models for replicative polymerases. Studies of mammalian polymerase δ from this laboratory (*6*, *15*) indicate that the behavior of mammalian polymerase δ is similar to that of T7$^-$ and RT in kinetic studies, thus validating use of T7$^-$ and RT as model polymerases to examine polymerase stalling caused by O^6-alkylG.

Polymerization Assays in the Presence of All Four dNTPs. Processive polymerization of T7$^-$ and RT was assessed using gel polymerization assays (Figure 1). Polymerization at and beyond O^6-MeG and O^6-BzG was analyzed using 24-mer/36-mer duplexes containing G, O^6-MeG, or O^6-BzG at position 25 (i.e., at the next available site of dNTP insertion). Increasing concentrations of T7$^-$ and RT were incubated for 30 min with each of the three primer/templates in the presence of all four dNTPs, permitting full-length synthesis.

Both polymerases fully extended the primer annealed to the unmodified DNA template with little difficulty (Figure 1). The product was one or two bases longer than the 36-mer template, indicating that blunt-end addition occurred. [Blunt-end addition during polymerization assays has been detected in previous studies from our laboratory for T7$^-$ and RT (*33*) and in other laboratories, e.g., ref *34*.] Polymerization on the 24-mer/36-O^6-MeG-mer by T7$^-$ and RT resulted in a ladder of intermediates with some full-length product. Polymerization on the 24-mer/36-O^6-MeG-mer yielded less extended primer when compared to the unmodified DNA substrate, indicating that the polymerases had some difficulty proceeding past the O^6-MeG. When T7$^-$ utilized 24-mer/36-O^6-BzG-mer as a substrate, polymerization was significantly inhibited when compared to the 24-mer/36-O^6-MeG-mer or the unmodified substrate. Accumulation of 25-mer product indicates that T7$^-$ stalled at the position one base beyond the site of the lesion. RT had even more difficulty utilizing 24-mer/36-O^6-BzG-mer as a substrate. Much of the starting primer was not extended, and there was significant accumulation of 25-mer and 26-mer product, indicating that RT stalled at positions one and two bases beyond O^6-BzG (i.e., RT had more difficulty forming full-length product using the 24-mer/36-O^6-BzG-mer substrate).

Phosphorothioate Analysis of Incorporation. In the pre-steady-state kinetic experiments performed in the rapid-quench flow instrument, DNA concentration exceeded enzyme concentration by 3-fold to examine a single reaction cycle (*5*, *29*). Enzyme and DNA were incubated to form E•DNA complexes, which were mixed with saturating dNTP-Mg^{2+} or dNTPαS-Mg^{2+} and then quenched following mixing times between 0.005 and 5 s (Figures 2 and 3). The first kinetic phase, i.e., the burst phase, was complete at ~100 ms for T7$^-$ and RT with each of the three different primer/template substrates, as determined by single-exponential analysis (*20*).

Pre-steady-state burst rates in the presence of dNTP and dNTPαS were compared to determine if the chemistry of phosphodiester bond formation is the rate-determining step during incorporation opposite O^6-alkylG. Incorporation of dCTPαS opposite guanine (i.e., 24-mer/36-G-mer) yielded either a 1.6-fold (T7$^-$) or 1.1-fold (RT) decrease in rate as compared to dCTP (Figures 2 and 3). During normal incorporation the conformational change, not the chemistry of bond formation, is generally accepted to be rate-limiting so only a small elemental effect is expected (*5*). Surprisingly, incorporation of sulfur-substituted nucleotides (i.e., dCTPαS or dTTPαS) into either the O^6-MeG-containing substrate or the O^6-BzG-containing substrate resulted in no more than a 2-fold decrease in the rate as compared to incorporation of unmodified nucleotides. During incorporation opposite some other DNA adducts, chemistry of bond formation is usually at least partially rate-limiting (*21*, *35*, *36*), but this was not the case during incorporation opposite O^6-alkylG.

Incorporation of either dCTP or dTTP opposite O^6-MeG and O^6-BzG resulted in a biphasic response (Figures 2 and 3). More significantly, the initial burst phase was not abolished during incorporation of phosphorothioate nucleotide analogue, a highly unusual occurrence (*15*, *35*). Thus,

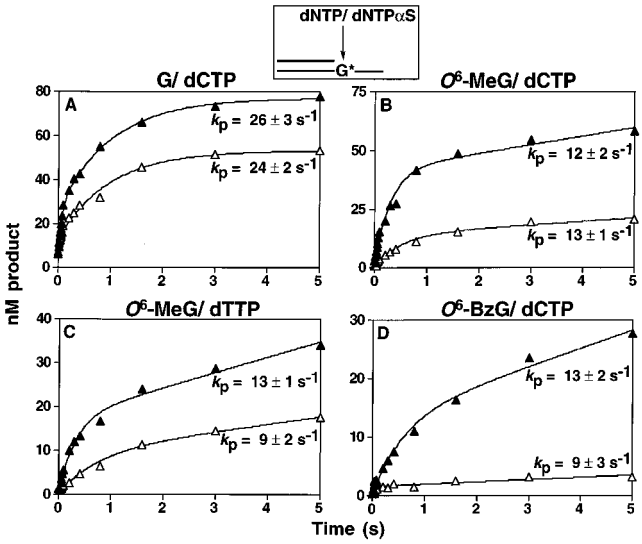

FIGURE 3: Phosphorothioate analysis of pre-steady-state kinetics of nucleotide incorporation by RT. (A) RT (69 nM) was incubated in the rapid quench-flow instrument with 100 nM 24-mer/36-G-mer to form an E•DNA complex. Mixing with 200 μM dCTP (▲) initiated the reaction. The pre-steady-state rate was determined from the burst equation, $y = A(1 - e^{-k_p t}) + k_{ss}t$, as described in the Experimental Procedures, and is indicated in the figure. RT (81 nM), incubated with 24-mer/36-G-mer, was mixed with 200 μM dCTPαS (△) to start the reaction. (B) RT (78 nM), preincubated with 100 nM 24-mer/36-O^6-MeG-mer, was mixed with 1.0 mM dCTP (▲) to begin polymerization. RT (72 nM) was incubated with 100 nM 24-mer/36-O^6-MeG-mer and mixed with 1.0 mM dCTPαS (△) to begin the reaction. (C) RT (140 nM), preincubated with 100 nM 24-mer/36-O^6-MeG-mer, was mixed with 1.0 mM dTTP (▲) to start the reaction. RT (60 nM) was mixed with 100 nM 24-mer/36-O^6-MeG-mer to form an E•DNA complex. Polymerization began upon addition of 1.0 mM dTTPαS (△). (D) RT (80 nM) was incubated with 100 nM 24-mer/36-O^6-BzG-mer and then mixed with 1.0 mM dCTP (▲), which initiated polymerization. RT (75 nM), preincubated with 100 nM 24-mer/36-O^6-BzG-mer, was mixed with 1.0 mM dCTPαS (△).

the results of the phosphorothioate analysis indicate that phosphodiester bond formation may not be rate-limiting during incorporation opposite O^6-alkylG, nor is it contributing significantly to the altered kinetics (i.e., nonstoichiometric burst amplitudes) (*20*) detected during misincorporation and stalling at O^6-MeG and O^6-BzG.

Determination of Productive DNA Binding, K_d^{DNA}, by Active Site Titration. Since polymerization is much faster than the dissociation of DNA from the polymerase, only preformed productive E•DNA complexes will form elongated product when polymerization is measured on a subsecond time-scale. If the change in burst amplitude is measured as a function of increasing DNA substrate concentration, the active site concentration of the enzyme can be determined. In addition, the K_d^{DNA} can be elucidated, a parameter that describes the dissociation constant of "productive" DNA binding.

T7$^-$ or RT was incubated with increasing concentrations of the substrate DNA to form an enzyme•DNA complex (Figures 4 and 5A,C). Each reaction was initiated by addition of saturating dCTP-Mg^{2+} and then quenched with 0.3 M EDTA after 0.15 s, to achieve maximal burst of polymerization with little contribution from multiple turnovers (*13*). The K_d^{DNA} for T7$^-$ with unmodified DNA was 19 ± 4 nM (Figure 4A), which is within the 5−20 nM range typical for

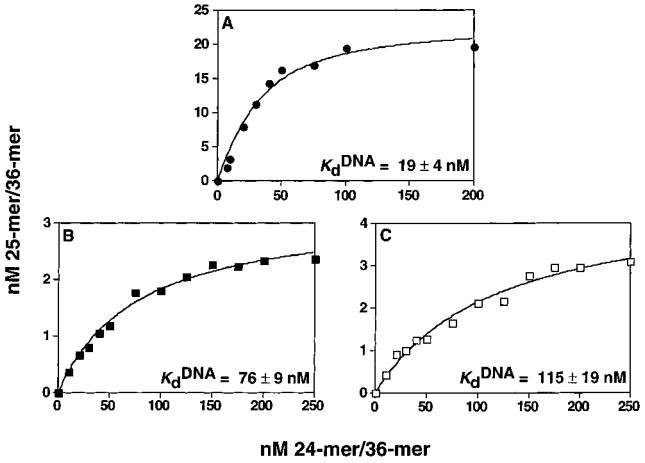

FIGURE 4: Determination of K_d^{DNA} with T7$^-$ by active site titration. The K_d^{DNA} for productive binding was determined by pre-steady-state analysis by comparing the maximal product formation as a function of DNA substrate concentration. (A) T7$^-$ (40 nM) was incubated with increasing 24-mer/36-G-mer concentrations (●, 7.5−200 nM) and mixed with 200 μM dCTP to initiate the reaction. Reactions were quenched with EDTA after 0.15 s. A graph of product formed (nM 25-mer/36-mer) vs starting concentration (nM 24-mer/36-mer) was plotted and was fit to a quadratic equation in Prism using the equation $[E•DNA] = 0.5(K_d + E_t + D_t) - [0.25\text{-}(K_d + E_t + D_t)^2 - E_tD_t]^{1/2}$ as described in the Experimental Procedures. (B) T7$^-$ (100 nM), preincubated with increasing 24-mer/36-O^6-MeG-mer concentrations (■, 10−250 nM), was mixed with 1.0 mM dCTP to begin polymerization. (C) T7$^-$ (100 nM) was mixed with increasing 24-mer/36-O^6-BzG-mer concentrations (□, 10−250 nM) to form an E•DNA complex. Reaction began upon addition of 1.0 mM dCTP.

unmodified DNA (*27*). The K_d^{DNA} for T7$^-$ productive binding of 24-mer/36-O^6-MeG-mer was approximately 4-fold higher than for unmodified DNA (Figure 4B) and 6-fold higher for 24-mer/36-O^6-BzG-mer (Figure 4C). Thus, the fraction of productive E•DNA complexes (i.e., complexes that can form product) of T7$^-$ with O^6-alkylG-containing substrates significantly decreases as compared to unmodified DNA.

As in the case of T7$^-$, the K_d^{DNA} for productive binding of unmodified DNA to RT was in the typical range seen with many polymerases, 18 ± 5 nM (Figure 5A). The K_d^{DNA} for RT doubled in the presence of the 24-mer/36-O^6-MeG-mer substrate (Figure 5C), and the K_d^{DNA} for the O^6-BzG-containing substrate was approximately 4-fold greater than that for unmodified DNA (Figure 5C). Since the determination of K_d^{DNA} is based on the ability of the E•DNA complex to form elongated product, the increase of the K_d^{DNA} in the presence of adducted substrates indicates a decrease in "productive" binding. This decreased productive binding indicates that when either T7$^-$ or RT binds an O^6-alkylG-containing substrate, the formation of productive complexes decreases as compared to the unmodified DNA substrate.

Estimation of Ground-State Binding, K_d. Active-site titrations allow determination of the K_d^{DNA} for productive binding but do not necessarily reflect ground-state binding of DNA to the polymerase, or vice versa. Fluorescence titrations (addition of RT to a solution of 18-FAM-mer/36-mer) were used to determine the ground-state binding of fluorescent DNA substrates to RT (Figure 5B, D). The environment of the fluorescent group is sensitive to the movement of RT as

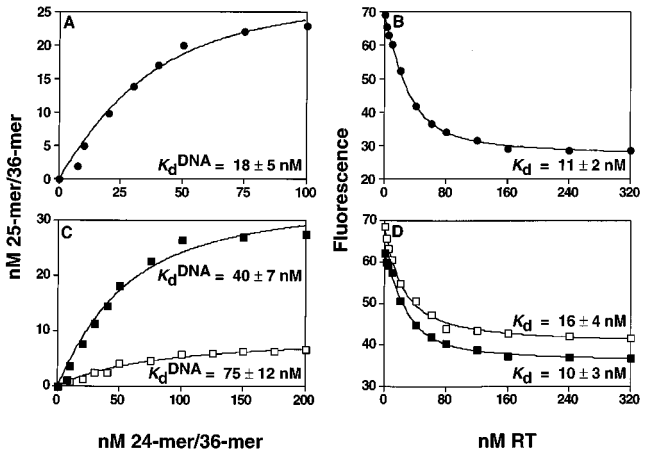

FIGURE 5: Comparison of K_d^{DNA} determined by active site titration vs K_d of ground-state binding estimated by fluorescence titration for RT. (A) RT (80 nM) was incubated with increasing 24-mer/36-G-mer concentrations (●, 7.5−100 nM) and mixed with 200 μM dCTP to initiate the reaction. Reactions were quenched with EDTA after 0.15 s. A graph of product formed (nM 25-mer/36-mer) vs starting concentration (nM 24-mer/36-mer) was plotted and was fit to a quadratic equation in Prism using the equation $[E•DNA] = 0.5(K_d + E_t + D_t) - [0.25(K_d + E_t + D_t)^2 - E_tD_t]^{1/2}$ as described in the Experimental Procedures. (B) RT (2.5 nM − 320 nM) was titrated into a solution of 50 nM 18-FAM-mer/36-G-mer (●). Fluorescence was monitored at an excitation wavelength of 492 nm and an emission wavelength of 516 nm. The data were fit to a fluorescence quadratic equation in Prism using the equation $E•DNA = F_o + (A/E_t)(0.5)[(K_d + E_t + D_t) - [(K_d + E_t + D_t)^{2-4*E_t*D_t}]^{1/2}]$ as described in the Experimental Procedures. (C) RT (100 nM) was preincubated with increasing 24-mer/36-O^6-MeG-mer concentrations (■, 7.5−200 nM) or increasing 24-mer/36-O^6-BzG-mer concentrations (□, 10−250 nM). The samples were mixed with 1.0 mM dCTP to initiate the reaction. (D) RT (2.5 nM − 320 nM) was titrated into a solution of 50 nM 18-FAM-mer/36-O^6-MeG-mer (■) or 18-FAM-mer/36-O^6-BzG-mer (□), and the change in fluorescence was monitored.

it binds its DNA substrate in the active site (*8*). RT contacts 18 base pairs of the duplex DNA substrate (*31*); thus, the 18-mer fluorescent primer should be within the DNA binding site of RT. The changes in the environment of 5′-FAM were monitored (excitation 492 nm, emission 516 nm), and fluorescence data were fit to a fluorescence quadratic equation to determine K_d.

The ground-state binding of the unmodified DNA substrate (i.e., 18-FAM-mer/36-G-mer) to RT was determined to be 11 ± 2 nM (Figure 5B), which is not significantly different from the K_d determined by active-site titration. Ground-state binding, i.e., K_d, for the adducted templates (Figure 5D) was very similar to that of the unmodified DNA, 10 ± 3 nM for O^6-MeG and 16 ± 4 nM for O^6-BzG. Thus, the ground-state binding of the adducted DNA substrates did not differ from the unmodified DNA substrate, indicating that the initial binding of the DNA to the polymerase (i.e., formation of E•DNA) is not significantly affected by the presence of O^6-alkylG in the active site.

Measurement of DNA Dissociation Rate, k_{off}. The dissociation rate of the E•DNA complex was determined using a DNA trapping experiment (Table 2). A preincubated solution of polymerase and unlabeled target DNA (either unmodified or adducted DNA) was mixed with ^{32}P-labeled 24-mer/36-G-mer for time intervals ranging from 0.08 to 30 s. After mixing for varying times, polymerization was initiated with dNTP-Mg^{2+} for a constant time of 0.25 s. (Any polymerase not bound to target DNA before mixing of E•DNA with labeled, trap DNA will elongate the trap DNA during the first 100 ms.) The reaction was quenched with EDTA to stop further polymerization, and the distribution of the polymerase between unlabeled target DNA and labeled (unmodified) DNA trap was determined. The increase in the amount of ^{32}P-labeled 25-mer/36-G-mer during the 250 ms corresponds to dissociation from the target DNA, and these results were fit to a single-exponential equation.

Table 2: Rates of DNA Dissociation from Polymerase, k_{off}

dissociating complex	T7$^-$ (s^{-1})	RT (s^{-1})
E•24/36-G	2.6 ± 0.5	1.0 ± 0.4
E•24/36-O^6-MeG	2.3 ± 0.3	1.2 ± 0.3
E•24/36-O^6-BzG	2.4 ± 0.6	1.4 ± 0.4
E•24dd/36-G•dCTP	0.5 ± 0.2	0.1 ± 0.04
E•24dd/36-O^6-MeG•dCTP	0.6 ± 0.2	0.05 ± 0.02
E•24dd/36-O^6-BzG•dCTP	0.7± 0.2	0.2 ± 0.04
E•24dd/36-G•dTTP	2.6 ± 0.5	0.8 ± 0.2

Dissociation of DNA from the RT•24-mer/36-G-mer complex occurred at a rate of 1.0 ± 0.4 s^{-1} (Table 2). The dissociation of O^6-MeG-containing-DNA and O^6-BzG-containing-DNA was similar to the dissociation rate of unmodified DNA, indicating that RT does not dissociate from adducted DNA more quickly than the unmodified substrate. Dissociation of DNA from a ternary complex of E•DNA•dNTP was measured using target DNA that contained a dideoxy-terminated primer (i.e., 24dd-mer, see Table 1), which prevents elongation of the DNA but allows formation of a stable ternary complex. Dissociation of DNA from RT•24dd-mer/36-G-mer•dCTP occurred at a rate of 0.10 ± 0.04 s^{-1}. Again, dissociation of O^6-alkylG-containing-DNA from E•DNA•dNTP complexes was not significantly different from dissociation of unmodified DNA from the ternary complex. DNA dissociation from the ternary complex was an order of magnitude slower than the dissociation of DNA from E•DNA. The dissociation of DNA from the ternary complex depended on the presence of the next correct nucleotide as dissociation of DNA from the RT•24dd-mer/36-G-mer•dTTP complex had a rate similar to that of the E•DNA complex. Thus, DNA dissociation rates from RT•DNA and RT•DNA•dNTP complexes did not increase in the presence of O^6-alkylG-containing DNA.

DNA dissociation from T7$^-$ occurred at a similar rate to that measured for RT. DNA dissociation from the T7$^-$•24-mer/36-G-mer complex[2] occurred at a rate of 2.6 ± 0.5 s^{-1} (Table 2), which was slightly faster than RT. This rate was similar to the rates of dissociation for E•DNA complexes containing modified DNA. This rate is approximately twice as fast as the dissociation of DNA from RT. Dissociation of DNA from T7$^-$•24dd-mer/36-G-mer•dCTP occurred at a rate of 0.5 ± 0.2 s^{-1} (Table 2). Again, dissociation of O^6-alkylG-containing-DNA from the E•DNA•dNTP complexes did not vary from the rate measured for the unmodified DNA substrate. Addition of the correct nucleotide stabilized the interaction of the polymerase with the DNA as the rate of

[2] A different preparation of T7$^-$ was used for the DNA dissociation experiments. All other experiments in this paper and the preceding paper in this issue (*20*) were done using T7$^-$ that had a pre-steady-state burst rate of 31 s^{-1} with a burst amplitude of 80% (see Figure 1 of ref *20*). The T7$^-$ used in the k_{off} experiments had a pre-steady-state burst rate of 26 s^{-1} with a burst amplitude of 57% (results not shown).

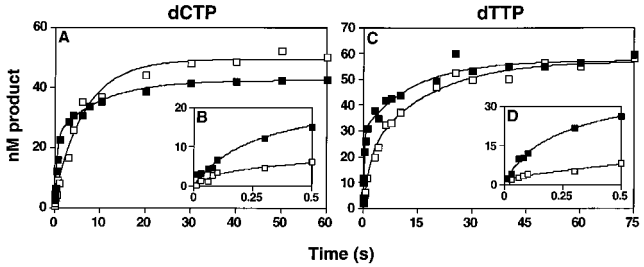

FIGURE 6: Pre-steady-state kinetics of RT with excess unlabeled DNA trap. (A) RT (88 nM) was incubated with 100 nM 24-mer/36-O^6-MeG-mer (■) in the rapid quench-flow apparatus and then mixed with 1.0 mM dCTP and excess unlabeled 24-mer/36-G-mer. Reactions were quenched with EDTA at various time intervals ranging from 0.01 to 75 s. A graph of nM product vs time was plotted, and the points were fit to a double-exponential equation in the Prism program, $y = E_tA_1(1 - e^{-k_1t}) + E_tA_2(1 - e^{-k_2t})$, as described in the Experimental Procedures. RT (81 nM) was preincubated with 100 nM 24-mer/36-O^6-BzG-mer (□). The E•DNA complex was mixed with 1.0 mM dCTP, in the presence of excess unlabeled 24-mer/36-G-mer, to initiate the reaction. (B) The reaction of RT with 24-mer/36-O^6-MeG-mer (■) or 24-mer/36-O^6-BzG-mer (□) has two different phases during the first 500 ms of the reaction; the first phase ends at ~100 ms. The two rates of incorporation opposite O^6-MeG were $k_1 = 15$ s^{-1} and $k_2 = 0.08$ s^{-1}; for O^6-BzG, $k_1 = 19$ s^{-1} and $k_2 = 0.07$ s^{-1}. (C) RT (52 nM) was mixed with 100 nM 24-mer/36-O^6-MeG-mer (■) or RT (91 nM) was mixed with 100 nM 24-mer/36-O^6-BzG-mer (□) to form an E•DNA complex. Polymerization was initiated by 1.0 mM dTTP in the presence of excess unlabeled 24-mer/36-G-mer. (D) The reaction of RT with 24-mer/36-O^6-MeG-mer (■) or 24-mer/36-O^6-BzG-mer (□) has two different phases during the first 500 ms of the reaction; the first phase ends at ~100 ms. The two rates of incorporation opposite O^6-MeG were $k_1 = 31$ s^{-1} and $k_2 = 0.05$ s^{-1} ; for O^6-BzG, $k_1 = 16$ s^{-1} and $k_2 = 0.04$ s^{-1}.

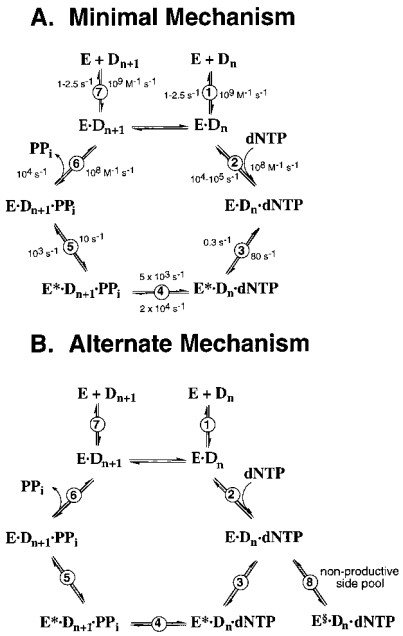

FIGURE 7: Kinetic mechanisms for DNA polymerase incorporation. Individual steps are numbered: E = polymerase, D_n = DNA substrate, E* = conformational change in polymerase, E§ = nonproductive conformation of polymerase, and D_{n+1} = DNA extended by one base. (A) Minimal kinetic mechanism of polymerization. Forward and reverse rate constants for each of the seven steps have been determined or are based on literature values for simulations of pre-steady-state kinetics of normal incorporation (*3*, *5*, *35*, *39*). (B) Alternate kinetic mechanism of polymerization for unusual replication substrates. An additional ternary complex forms, which is catalytically incompetent.

dissociation for the E•DNA•dNTP complex was 5-fold less than that of the E•DNA complex. This decrease in k_{off} depended on the presence of the correct nucleotide as the T7$^-$•24dd-mer/36-G-mer•dTTP complex had a rate similar to that of the binary complex. Thus, regardless of the polymerase, DNA dissociation from E•DNA and E•DNA• dNTP complexes occurred at similar rates for unmodified and adducted DNA.

Pre-Steady-State Kinetics at DNA Adducts in the Presence of Trap DNA (Single-Turnover Experiments). Experiments were designed to restrict analysis of polymerization to the initial reaction cycle in order to avoid observation of phenomena occurring after interaction of polymerase with DNA, i.e., dissociation and reassociation of polymerase and DNA (*13*, *14*). During DNA trap experiments, preequilibrated RT•DNA complex was mixed with dNTP-Mg^{2+} in the presence of excess unlabeled 24-mer/36-G-mer (Figure 6). Reactions were quenched with 0.3 M EDTA at time intervals ranging from 0.01 to 75 s, and the results were fit to a biphasic equation. RT incorporation of dCTP at O^6-MeG was biphasic, and the rates of the two phases differed by 2 orders of magnitude. Incorporation of dCTP opposite O^6-MeG occurred at a fast rate (k_1) of 15 s^{-1} (during the first 100 ms) with a second slower rate (k_2) of 0.08 s^{-1} (Figure 6A). Incorporation of dCTP opposite O^6-BzG exhibited similar kinetics to that of O^6-MeG; incorporation of dTTP across from both O^6-MeG and O^6-BzG also behaved similarly (Figure 6C). During the first 500 ms of the reaction (Figure 6B,D) two phases of polymerization were detected: a rapid initial burst followed by a second slower phase. The second slower phase cannot be dictated by DNA dissociation as in normal pre-steady-state kinetics (see Figures 2 and 3) due to the inclusion of excess unlabeled DNA.

Trap experiments performed with RT and 24-mer/36-G-mer also yielded biphasic kinetics similar to those seen for O^6-MeG and O^6-BzG (results not shown), but the second rate (k_2) was 0.4 s^{-1}, which is only an order magnitude slower than the fast, first rate (k_1). RT has the ability to form nonproductive complexes with unmodified DNA, but these complexes can change conformation to become complexes competent for chemistry of phosphodiester bond formation (*19*). Thus, the existence of a slower polymerization rate (k_2) in the presence of a DNA trap corresponds to a second pool of polymerase complexes that have changed conformation to undergo chemistry of bond formation. The second rate of incorporation (k_2) opposite O^6-MeG and O^6-BzG was about 2 orders of magnitude slower than the initial, fast rate. This very slow second rate (as compared to that seen with unmodified DNA) indicates that the ability of these nonproductive complexes to change conformation and undergo chemistry of bond formation is greatly hindered by the presence of O^6-alkylG at the active site of the polymerase.

DISCUSSION

The mechanism of polymerase fidelity has been the subject of intense interest since the discovery of the first polymerase by Kornberg in 1956 (*37*, *38*). Following the elucidation of the detailed kinetic mechanism of incorporation (*3*, *5*) (Figure 7A), considerable attention has been given to the role of the rate-limiting conformational change in the maintenance of

polymerase fidelity. Crystal structures of numerous polymerases have produced evidence for an "induced fit" mechanism as a rigorous check for formation of correct Watson−Crick base pairs (*8*, *9*, *40*). The formation of a correct base pair between an incoming dNTP and the DNA substrate (i.e., correct Watson−Crick geometry in the polymerase active site) readily induces the rate-limiting conformational change, thus aligning the substrates for catalysis, whereas an incorrect base pair does not (*40*). Crystal structures of E•DNA•dNTP complexes have supported the kinetic evidence for this seemingly important rate-limiting conformational change, although recent evidence on the role of Mg^{2+} binding with polymerase β suggests that our understanding of the conformational change may be too simplistic (*41*, *42*).

The kinetics of incorporation with normal DNA substrates have been rigorously studied (*3*-*6*, *43*). A polymerase encounter with a DNA−carcinogen adduct perturbs polymerase fidelity (*44*), and the normal mechanism for fidelity often fails to prevent incorporation of the incorrect nucleotide. Changes in the equilibrium/rates of various steps of the minimal mechanism of incorporation (Figure 7A) have been proposed to occur in the presence of DNA-carcinogen adducts. In this study, the pre-steady-state kinetics of T7$^-$ and RT with O^6-MeG and O^6-BzG were examined in order to understand how DNA adducts perturb polymerase enzymology, thus allowing misincorporations.

Proposed Changes in the Minimal Mechanism to Explain Kinetics at DNA Adducts. Polymerase assays done in the presence of all four dNTPs (Figure 1) qualitatively demonstrate that T7$^-$ and RT had difficulty incorporating any nucleotide opposite O^6-MeG and O^6-BzG, as indicated by accumulation of several intermediates. Both T7$^-$ and RT stalled more in the presence of O^6-BzG than O^6-MeG, suggesting that O^6-BzG is more of a hindrance to processive polymerization than O^6-MeG. Detailed pre-steady-state kinetic analysis indicated that the "stalling" (i.e., accumulation of intermediates) accessed by gel electrophoresis occurred because the rapid burst kinetics of normal incorporation were greatly attenuated in the presence of a DNA adduct (*20*).

Previous studies with DNA adducts have shown that (*S*p)-dNTPαS substitution for dNTP causes a 100-fold decrease in the rate. This decrease in rate may indicate that the chemistry of bond formation has become the rate-limiting step, rather than the preceding conformational change (*5*, *21*, *35*, *45*−*47*). There has been some controversy in the literature regarding the meaning of the elemental thio effect. A paper by Herschlag et al. (*48*) raised some doubts of the interpretation of some previously published thio effects; however, hydrolysis of phosphodiesters by ribozymes may not behave exactly like polymerization reactions. The problem with interpreting the thio effect is that the magnitude of the elemental effect depends on the transition state, which may vary.

Eger and Benkovic (*49*) demonstrated that the dNTPαS binds the polymerase much like unmodified dNTP, thus eliminating nucleotide binding as the source of the experimentally observed thio effect. Although the thio effect is not a direct measure of the chemistry step of bond formation, steps after dNTP binding play a significant role in the determination of the rate. Although changes in the conformational change could also contribute to the thio effect, chemistry does play some role. It is possible that the dNTPαS influences the juxtaposition of the atoms, thus affecting something other than chemistry.

Despite the controversy, many groups have noted significant thio effects in the presence of a mispair (*47*) and O^6-MeG (*35*). In fact, several studies from our laboratory with the same sequence have noted significant elemental effects (up to 150) with 8-oxoG by T7$^-$ and RT (*21*, *46*) and by polymerase δ (*15*). In contrast to the results obtained in numerous studies, a very small thio effect was noted for T7$^-$ and RT in the presence of O^6-alkylG (Figures 2 and 3). Also, (S_p)-dNTPαS substitution for dNTP did not abolish the burst kinetics as was seen with other DNA adducts (*15*, *21*, *35*, *46*). Although phosphorothioate analysis of incorporation may not be a direct measure of bond formation, thio analysis of O^6-alkylG was strikingly different from studies of other adducts, which may indicate that the chemistry of bond formation (Figure 7A, step 4) is not significantly affected during incorporation opposite O^6-alkylG.

Others have suggested that polymerases have lower affinity for carcinogen-adducted DNA (*50*−*52*); therefore, increased dissociation of the DNA substrate (k_{off}) could possibly explain the altered kinetics of incorporation opposite O^6-MeG and O^6-BzG (Figure 7A, step 7). DNA dissociation from E•DNA did not increase when the polymerase bound an O^6-alkylG-containing substrate (as compared to the unmodified substrate). The k_{off} for T7$^-$ was about twice as fast as the rate for RT. This result was not surprising because the steady-state rate for T7$^-$ was also about 2-fold faster than the steady-state rate for RT (*20*), and it is generally believed that the DNA dissociation from the polymerase is the overall rate-limiting step and determines rates measured under steady-state conditions (*3*, *5*). Although the dissociation rate is an order of magnitude faster than the steady-state rate, the steady-state rate may not necessarily be equal to the rate of a single step in the cycle because some of the reverse reactions of polymerization contribute to the steady-state rate (*53*). Nevertheless, the constancy of the k_{off} rates indicates that increased DNA dissociation is not a factor during incorporation opposite O^6-alkylG.

The ground-state binding of the DNA to the polymerase, K_d, (Figure 7A, step 1) was determined by fluorescence titrations (Figure 5B,D). The presence of O^6-alkylG in the active site of RT did not change the K_d, indicating that initial binding of DNA to the polymerase to form E•DNA was not affected by the presence of the DNA lesion. Interestingly, the active site titrations indicate that when T7$^-$ or RT binds an O^6-alkylG-containing substrate, the K_d^{DNA} increases significantly with respect to an unmodified DNA substrate (Figures 4 and 5A,C). Since determination of K_d^{DNA} is governed by product formation (Figure 7A, step 4), a decreased ability to form product indicates decreased productive binding of the substrate. Also, the ability to form product correlates with the number of catalytically competent polymerase complexes (*27*). Thus, an O^6-alkylG in the active site results in the formation of fewer productive complexes.

Nonproductive Polymerase Complex to Explain Altered Kinetics at DNA Adducts. As discussed previously, neither increased DNA dissociation, a decreased DNA binding affinity, nor slower chemistry of bond formation can explain the altered kinetics of misincorporation nor do they explain why fewer productive complexes are formed with adducted

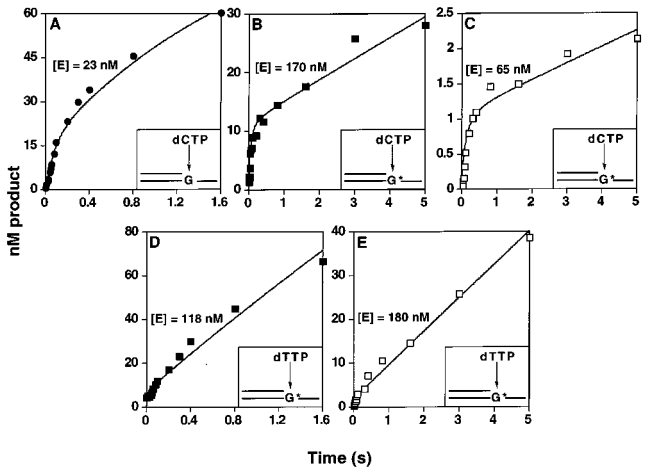

FIGURE 8: Simulation of pre-steady-state burst kinetics of incorporation opposite G (●), O^6-MeG (■), or O^6-BzG (□) by T7$^-$. Symbols represent experimentally determined incorporation, and the solid lines represent simulations of the results by the minimal mechanism (Figure 7A) or the alternate mechanism (Figure 7B) using the rate constants shown in Figure 7A and Table 3. (A) T7$^-$ (23 nM) was incubated with 100 nM 24-mer/36-G-mer in the rapid quench-flow instrument and mixed with 200 μM dCTP−Mg^{2+} to initiate the reaction. The solid line represents the simulation of the results using the minimal mechanism whereas all other lines (B−E) represent simulations using the alternate mechanism. (B) T7$^-$ (170 nM), preincubated with 250 nM 24-mer/36-O^6-MeG-mer, was mixed with 2.0 mM dCTP−Mg^{2+} to begin polymerization. (C) T7$^-$ (65 nM) was incubated with 100 nM 24-mer/36-O^6-BzG-mer and mixed with 1.0 mM dCTP-Mg^{2+}. (D) T7$^-$ (118 nM) was incubated with 250 nM 24-mer/36-O^6-MeG-mer. The reaction was started with addition of 1.0 mM dTTP-Mg^{2+}. (E) T7$^-$ (180 nM) formed a binary complex with 250 nM 24-mer/36-O^6-BzG-mer. To begin the reaction, 3.0 mM dTTP-Mg^{2+} was added. All reactions were quenched at the specified times using 0.3 M EDTA.

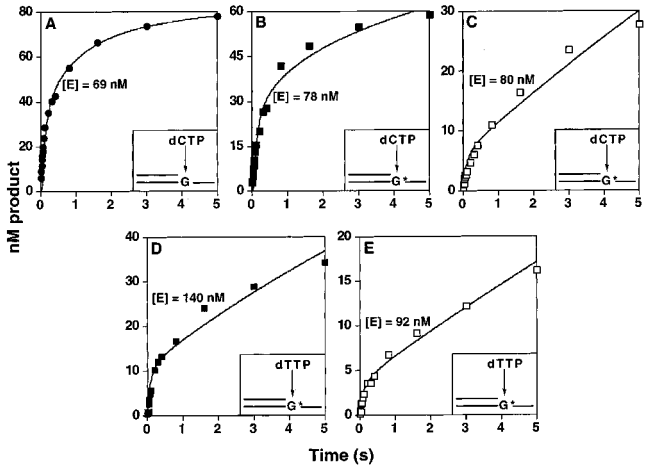

FIGURE 9: Simulation of pre-steady-state burst kinetics of incorporation opposite G (●), O^6-MeG (■), or O^6-BzG (□) by RT. Symbols represent experimentally determined incorporation, and the solid lines represent simulations of the results by the alternate mechanism (Figure 7B) using the rate constants shown in Figure 7A and Table 3. (A) RT (69 nM) was incubated with 100 nM 24-mer/36-G-mer in the rapid-quench flow apparatus, and 200 μM dCTP-Mg^{2+} was added to initiate reaction. (B) RT (78 nM), preincubated with 100 nM 24-mer/36-O^6-MeG-mer, was mixed with 1.0 mM dCTP−Mg^{2+} to begin polymerization. (C) RT (80 nM) was mixed with 100 nM 24-mer/36-O^6-BzG-mer. To begin the reaction, 1.0 mM dCTP-Mg^{2+} was added. (D) RT (140 nM) formed a binary complex with 100 nM 24-mer/36-O^6-MeG-mer, and addition of 1.0 mM dTTP-Mg^{2+} initiated polymerization. (E) RT (92 nM) was incubated with 100 nM 24-mer/36-O^6-BzG-mer and then mixed with 1.0 mM dTTP-Mg^{2+}. All reactions were quenched with EDTA at the indicated times.

DNA. Pre-steady-state experiments in the presence of trap DNA reveal two rates of incorporation at DNA adducts that differ by 2 orders of magnitude (Figure 6). The minimal mechanism of nucleotide incorporation (Figure 7A) consists of one pathway of bond formation that occurs at a rate dependent on the conformational change (step 3) and bond formation (step 4). Changes in individual rates of the minimal mechanism cannot explain the substoichiometric burst amplitudes (*20*), the two rates of incorporation at DNA adducts, or the existence of fewer productive complexes at O^6-alkylG.

To explain the kinetics observed during incorporation opposite a DNA adduct, an alternate mechanism must be proposed (Figure 7B) in which an additional E•DNA•dNTP complex has been included (Figure 7B, step 8) that is not catalytically competent. This nonproductive ternary complex can feed back into the cycle, following a conformational change to a productive complex, to then undergo chemistry of bond formation. The existence of this nonproductive side pool readily explains the two rates of incorporation at DNA adducts (Figure 6) because the second, slower rate corresponds to the nonproductive complex completing bond formation after it becomes catalytically active.

To access the feasibility of this alternate mechanism, kinetic simulations were performed [using the program DynaFit (*30*)], a modeling technique that has been used by many groups to analyze the minimal mechanism of incorporation (*3*−*5*, *19*, *21*, *39*). Although kinetic simulations cannot prove that a mechanism actually occurs, it can readily eliminate invalid mechanisms that cannot simulate the experimentally determined results. For incorporation of dCTP opposite G by T7$^-$, simulation of the experimental results using the minimal mechanism with the rates shown (Figure 7A) yielded a reasonable fit (Figure 8A) of the nearly stoichiometric burst amplitude (82%) (*20*). As expected, formation of a normal Watson−Crick base pair is controlled by the rate-limiting conformational change (Figure 7A, step 3).

Although the minimal mechanism describes the kinetics of T7$^-$ incorporation using normal DNA substrates, it failed to adequately simulate the kinetics of incorporation of either dCTP or dTTP opposite O^6-alkylG by T7$^-$ and RT (results not shown). During incorporation opposite either O^6-MeG or O^6-BzG, the substoichiometric burst amplitudes ranged from 2 to 28% of the expected amplitude (*20*) with respect to enzyme concentration (determined by UV). Adjusting the rates of bond formation (k_4), conformational change (k_3), and DNA dissociation (k_7) did not yield a reasonable fit of the experimentally determined results. Interestingly, a somewhat reasonable fit of the results could be generated by artificially lowering the enzyme concentration to that of the burst amplitude. It should be noted that while lowering the enzyme concentration could yield an adequate fit of the burst phase to the minimal mechanism, the slower second phase of the reaction deviated from the simulated curve.

The alternate mechanism, which contains a nonproductive ternary complex (Figure 7B), was used to simulate the pre-steady-state kinetics of incorporation opposite O^6-alkylG by T7$^-$ and RT (Figures 8 and 9). In every case, the alternate mechanism yielded a reasonable fit to the experimental results using the actual enzyme concentration. [The alternate

Table 3: Computer Kinetic Modeling of Pre-Steady-State Rate Constants

enzyme	dNTP inserted	template	EDN ↔ E*DN k_3[a] (s^{-1})	E*DN ↔ E§DN k_8 (s^{-1})	E*DN ↔ E§DN k_{-8} (s^{-1})
T7⁻	**dCTP**	G	90 ± 5		
		O^6-MeG	26 ± 1	370 ± 20	0.33 ± 0.04
		O^6-BzG	23 ± 1	1300 ± 90	0.2 ± 0.04
	dTTP	O^6-MeG	18 ± 2	300 ± 70	7 ± 2
		O^6-BzG	17 ± 1	1800 ± 430	5 ± 1
RT	**dCTP**	G	81 ± 9	29 ± 5	0.1 ± 0.03
		O^6-MeG	49 ± 2	67 ± 5	0.2 ± 0.04
		O^6-BzG	42 ± 2	380 ± 30	0.6 ± 0.1
	dTTP	O^6-MeG	25 ± 1	190 ± 10	0.6 ± 0.1
		O^6-BzG	47 ± 1	910 ± 60	0.7 ± 0.2

[a] Indicated rates and errors were estimated using DynaFit.

mechanism also yielded reasonable fits to kinetics observed for next-base extension following an O^6-alkylG:C or an O^6-alkylG:T base pair (results not shown).] Although the rate of bond formation (k_4) was varied over a wide range, changing the value of k_4 did not improve the fit to the experimental results. Thus, the rate constants used in the simulation did not vary from those of the minimal mechanism (Figure 7A), with the exception of k_3 (Table 3).

The value of k_3, which measures the rate of the conformational change, decreased 2 to 4-fold during incorporation opposite O^6-alkylG, as compared to normal incorporation (Table 3). The inability to fit the experimental results to a simulation of the minimal mechanism indicates that this small change in k_3 cannot fully account for the large attenuation in the burst amplitude. More significantly, the simulated values for k_8 varied greatly, from 67 to 1800 s^{-1}. Thus, the formation of the nonproductive ternary complex occurs at a very fast rate in the presence of a DNA adduct, but the actual rate depends on the adduct structure. The fastest rates of formation of the nonproductive complex were observed for incorporation opposite O^6-BzG. The fast formation of a nonproductive complex in the presence of O^6-BzG correlates with the increased polymerase stalling at the site of this adduct, which was observed during processive polymerization (Figure 1) and in pre-steady-state kinetics, i.e., the very small burst amplitudes (*20*).

Return of the nonproductive complex to the main portion of the cycle, via a conformational change to become a catalytically competent ternary complex, is controlled by the value of k_{-8}. The isomerization of the nonproductive complex to form a complex poised for chemistry was significantly slower than any other step in the cycle (Table 3, Figure 7A) and becomes the rate-limiting step during the incorporation opposite a DNA adduct. Since the rate of this step (k_{-8}) is slower than the dissociation of the DNA from the polymerase (k_7), DNA dissociation from the E•DNA complex is not governing the steady-state rate as it does during normal incorporation. Interestingly, DNA dissociation from the ternary complex (Table 2) is somewhat similar to k_{-8}. Thus, dissociation of the DNA from the nonproductive ternary complex may compete with formation of the catalytically competent complex and subsequently also contribute to the steady-state rate of incorporation opposite an adduct. In addition, the value of k_{-8} is somewhat similar to the second, slower rate of incorporation (k_2) determined in the presence of a DNA trap (Figure 6). In this experiment, product formation plateaus at 50 nM, which may be due to the competition between product formation (via formation of a catalytically competent ternary complex, k_{-8}) and dissociation of DNA from the nonproductive ternary complex.

The incorporation of dCTP opposite the normal base G by RT seems to be an exception to the trend because it could not be fit to the minimal mechanism (Table 3). Other groups have observed nonproductive binding of normal DNA by RT (*19*), and the propensity of RT to bind its DNA substrate in a nonproductive manner has even required special techniques to obtain meaningful crystal structures (*8*). Thus, it is not surprising that normal incorporation by RT could only be simulated by the alternate mechanism; however, the rate of the conformational change (k_3) was similar to that of normal incorporation by T7⁻. Also, the predicted value of k_8 was significantly lower than those predicted for incorporation opposite O^6-alkylG, indicating that RT does not form nonproductive complexes as readily with normal DNA as it does with modified DNA.

Evidence for a Nonproductive Complex at Other DNA Adducts. Several other studies, including one from our laboratory, have also proposed that the minimal mechanism does not sufficiently explain the altered kinetics observed at unusual DNA substrates, such as DNA secondary structures (*11*), DNA−carcinogen adducts of widely varying structure (*13*, *14*), and natural "pause" sites (*12*, *19*). Suo et al. (*13*) proposed that an alternate E•DNA complex existed in equilibrium with the catalytically competent binary complex when either T7⁻ or RT attempted to replicate DNA containing a cisplatin adduct. This mechanism contrasts with our mechanism, which includes an alternate ternary complex rather than a binary complex. Measuring the K_d^{dNTP} for incorporation by RT (*20*) indicated that the formation of the productive ternary complex was hindered in the presence of a DNA adduct as the productive binding of the dNTP decreased (i.e., severalfold increase in K_d^{dNTP}) as compared to unmodified DNA. As Suo et al. (*13*) proposed, an alternate E•DNA complex could explain this decreased dNTP binding affinity. Although the K_d^{dNTP} increased greatly in the presence of an adduct, formation of the ternary complex resulted in a decreased rate of DNA dissociation (Table 2), indicating that the dNTP stabilizes the E•DNA complex. Thus, it seems that the initial ternary complex may be readily formed, but one of the subsequent steps is perturbed. Thus, our proposed alternate mechanism contains a nonproductive ternary complex, but the existence of an additional E•DNA complex must also be considered.

Previous work from this laboratory examined the insertion of dATP opposite 8-oxoG, as well as incorporation of 8-oxodGTP into normal DNA, by RT (*14*, *21*, *28*). Incorporation opposite a template 8-oxoG and insertion of the modified nucleotide yielded pre-steady-state kinetics with substoichiometric bursts. The validity of three alternate mechanisms was considered by evaluating kinetic simulations of each of these mechanisms to the experimental results. These mechanisms contain additional complexes, including a nonproductive ternary complex, a nonproductive binary complex that can bind nucleotide, and an additional productive ternary complex that is not kinetically favorable. All mechanisms produced reasonable fits to the experimental results and are valid explanations of the altered kinetics

observed for incorporation opposite DNA−carcinogen adducts or for incorporation of modified nucleotides. More experiments will be required to characterize additional complexes formed when polymerases attempt to replicate unusual substrates.

Overall, the experimental results and kinetic simulations strongly indicate that the minimal mechanism of incorporation (Figure 7A) does not sufficiently describe the altered kinetics detected during a polymerase encounter with DNA−carcinogen adducts. The substoichiometric burst amplitudes, the two rates of incorporation opposite the DNA lesions, and the existence of fewer productive complexes in the presence of O^6-alkylG suggest that incorporation opposite DNA adducts can be more accurately explained by a mechanism that includes a nonproductive complex. Interestingly, a helix-distorting cisplatin adduct (*13*) and the small but mutagenic 8-oxoG adduct (*14*) exhibit kinetics that are similar to those detected at O^6-alkylG. Thus, DNA adducts of varied structure with different biological effects can cause alternate conformations in enzyme, DNA, or nucleotide, which may contribute to the formation of a nonproductive binary or ternary complex. In conclusion, polymerase stalling at O^6-alkylG produces altered kinetics as compared to normal incorporation, and these kinetics are best described by the existence of an additional polymerase complex.

ACKNOWLEDGMENT

We thank M.-S. Kim, L. Nechev, C. M. Harris, P. Tamura, H. Shimamura, and J. B. Wheeler for help in synthesis and characterization of the O^6-Bz-dG-containing 36-mer. We also thank S. Langouët, L. L. Furge, and H. J. Einolf for assistance in protein purification and kinetic analysis. Finally, we thank K. A. Johnson and A. A. Johnson for their advice on the DNA dissociation (k_{off}) experiments.

SUPPORTING INFORMATION AVAILABLE

Two examples of DynaFit scripts used to model the experimental data. Incorporation of dCTP opposite G by $T7^-$ was simulated using the minimal mechanism (Figure 7A), while all other reactions yielded a more reasonable simulation using the alternate mechanism (Figure 7B), which includes a nonproductive ternary complex. This information is available free of charge via the Internet at http://pubs.acs.org.

REFERENCES

1. Loeb, L. A. (1991) *Cancer Res. 51*, 3075−3079.
2. Baker, T. A., and Bell, S. P. (1998) *Cell 92*, 295−305.
3. Kuchta, R. D., Mizrahi, V., Benkovic, P. A., Johnson, K. A., and Benkovic, S. J. (1987) *Biochemistry 26*, 8410−8417.
4. Kati, W. M., Johnson, K. A., Jerva, L. F., and Anderson, K. S. (1992) *J. Biol. Chem. 267*, 25988−25997.
5. Patel, S. S., Wong, I., and Johnson, K. A. (1991) *Biochemistry 30*, 511−525.
6. Einolf, H. J., and Guengerich, F. P. (2000) *J. Biol. Chem. 275*, 16316−16322.
7. Johnson, K. A. (1993) *Annu. Rev. Biochem. 62*, 685−713.
8. Huang, H., Chopra, R., Verdine, G. L., and Harrison, S. C. (1998) *Science 282*, 1669−1675.
9. Doublié, S., Tabor, S., Long, A. M., Richardson, C. C., and Ellenberger, T. (1998) *Nature 391*, 251−257.
10. Steitz, T. A. (1998) *Nature 391*, 231−232.
11. Suo, Z., and Johnson, K. A. (1998) *J. Biol. Chem. 273*, 27259−27267.
12. Suo, Z., and Johnson, K. A. (1997) *Biochemistry 36*, 12459−12467.
13. Suo, Z., Lippard, S. J., and Johnson, K. A. (1999) *Biochemistry 38*, 715−726.
14. Furge, L. L., and Guengerich, F. P. (1999) *Biochemistry 38*, 4818−4825.
15. Einolf, H. J., and Guengerich, F. P. (2001) *J. Biol. Chem. 276*, 3764−3771.
16. Klarmann, G. J., Schauber, C. A., and Preston, B. D. (1993) *J. Biol. Chem. 268*, 9793−9802.
17. Friedberg, E. C., and Gerlach, V. L. (1999) *Cell 98*, 413−416.
18. Goodman, M. F. (1998) *Nature 395*, 221−223.
19. Wöhrl, B. M., Krebs, R., Goody, R. S., and Restle, T. (1999) *J. Mol. Biol. 292*, 333−344.
20. Woodside, A. M., and Guengerich, F. P. (2002) *Biochemistry 41*, 1027−1038.
21. Furge, L. L., and Guengerich, F. P. (1997) *Biochemistry 36*, 6475−6487.
22. Lunn, C. A., Kathju, S., Wallace, B. J., Kushner, S. R., and Pigiet, V. (1984) *J. Biol. Chem. 259*, 10469−10474.
23. Le Grice, S. F. J., Cameron, C. E., and Benkovic, S. J. (1995) *Methods Enzymol. 262*, 130−144.
24. Borer, P. N. (1975) in *Handbook of Biochemistry and Molecular Biology, 3rd ed* (Fasman, G. D., Ed.) pp 589−590, CRC Press, Cleveland, OH.
25. Kim, M.-S., and Guengerich, F. P. (1997) *Chem. Res. Toxicol. 10*, 1133−1143.
26. Huber, H. E., Tabor, S., and Richardson, C. C. (1987) *J. Biol. Chem. 262*, 16224−16232.
27. Johnson, K. A. (1995) *Methods Enzymol. 249*, 38−61.
28. Einolf, H. J., Schnetz-Boutaud, N., and Guengerich, F. P. (1998) *Biochemistry 37*, 13300−13312.
29. Mizrahi, V., Henrie, R. N., Marlier, J. F., Johnson, K. A., and Benkovic, S. J. (1985) *Biochemistry 24*, 4010−4018.
30. Kuzmic, P. (1996) *Anal. Biochem. 237*, 260−273.
31. Jacobo-Molina, A., Ding, J., Nanni, R. G., Clark, A. D., Jr., Lu, X., Tantillo, C., Williams, R. L., Kamer, G., Ferris, A. L., Clark, P., Hizi, A., Hughes, S. H., and Arnold, E. (1993) *Proc. Natl. Acad. Sci. U.S.A. 90*, 6320−6324.
32. Zinnen, S., Hsieh, J. C., and Modrich, P. (1994) *J. Biol. Chem. 269*, 24195−24202.
33. Langouët, S., Mican, A. N., Müller, M., Fink, S. P., Marnett, L. J., Muhle, S. A., and Guengerich, F. P. (1998) *Biochemistry 37*, 5184−5193.
34. Patel, P. H., and Preston, B. D. (1994) *Proc. Natl. Acad. Sci. U.S.A. 91*, 549−553.
35. Tan, H. B., Swann, P. F., and Chance, E. M. (1994) *Biochemistry 33*, 5335−5346.
36. Lowe, L. G., and Guengerich, F. P. (1996) *Biochemistry 35*, 9840−9849.
37. Kornberg, A., Lehman, I. R., Bessman, M. J., and Simms, E. S. (1956) *Biochim. Biophys. Acta 21*, 197−198.
38. Lehman, I. R., Bessman, M. J., Simms, E. S., and Kornberg, A. (1958) *J. Biol. Chem. 233*, 163−170.
39. Hsieh, J.-C., Zinnen, S., and Modrich, P. (1993) *J. Biol. Chem. 268*, 24607−24613.
40. Sawaya, M. R., Prasad, R., Wilson, S. H., Kraut, J., and Pelletier, H. (1997) *Biochemistry 36*, 11205−11215.
41. Zhong, X., Patel, S. S., Werneburg, B. G., and Tsai, M. D. (1997) *Biochemistry 36*, 11891−11900.
42. Arndt, J. W., Gong, W., Zhong, X., Showalter, A. K., Liu, J., Dunlap, C. A., Lin, Z., Paxson, C., Tsai, M. D., and Chan, M. K. (2001) *Biochemistry 40*, 5368−5375.
43. Johnson, A. A., Tsai, Y., Graves, S. W., and Johnson, K. A. (2000) *Biochemistry 39*, 1702−1708.
44. Echols, H., and Goodman, M. F. (1991) *Annu. Rev. Biochem. 60*, 477−511.
45. Eckstein, F. (1985) *Annu. Rev. Biochem. 54*, 367−402.
46. Furge, L. L., and Guengerich, F. P. (1998) *Biochemistry 37*, 3567−3574.
47. Wong, I., Patel, S. S., and Johnson, K. A. (1991) *Biochemistry 30*, 526−537.

48. Herschlag, D., Piccirilli, J. A., and Cech, T. R. (1991) *Biochemistry 30*, 4844−4854.
49. Eger, B. T., and Benkovic, S. J. (1992) *Biochemistry 31*, 9227−9236.
50. Forgacs, E., Latham, G., Beard, W. A., Prasad, R., Bebenek, K., Kunkel, T. A., Wilson, S. H., and Lloyd, R. S. (1997) *J. Biol. Chem. 272*, 8525−8530.
51. Alekseyev, Y. O., Dzantiev, L., and Romano, L. J. (2001) *Biochemistry 40*, 2282−2290.
52. Rechkoblit, O., Amin, S., and Geacintov, N. E. (1999) *Biochemistry 38*, 11834−11843.
53. Northrop, D. B. (1998) *J. Chem. Educ. 75*, 1153−1157.

BI011496F